HHS Public Access

Author manuscript

Sci Immunol. Author manuscript; available in PMC 2021 November 11.

Published in final edited form as:

Sci Immunol. 2020 July 24; 5(49): . doi:10.1126/sciimmunol.abc9492.

Absence of mucosal-associated invariant T cells in a person with a homozygous point mutation in *MR1*

Lauren J. Howson[1,*], **Wael Awad**[1,2], **Anouk von Borstel**[1], **Hui Jing Lim**[3], **Hamish E.G. McWilliam**[3,4], **Maria L. Sandoval-Romero**[1], **Shamik Majumdar**[5], **Abdul R. Hamzeh**[6,7], **Thomas D. Andrews**[6,7], **David H. McDermott**[5], **Philip M. Murphy**[5], **Jérôme Le Nours**[1,2], **Jeffrey Y.W. Mak**[8,9], **Ligong Liu**[8,9], **David P. Fairlie**[8,9], **James McCluskey**[3], **Jose A. Villadangos**[3,4], **Matthew C. Cook**[6,7], **Stephen J. Turner**[10], **Martin S. Davey**[1,†], **Samar Ojaimi**[11,12,†], **Jamie Rossjohn**[1,2,13,*]

[1]Infection and Immunity Program and Department of Biochemistry and Molecular Biology, Biomedicine Discovery Institute, Monash University, Clayton, Victoria, Australia

[2]Australian Research Council Centre of Excellence in Advanced Molecular Imaging, Monash University, Clayton, Victoria, 3800, Australia

[3]Department of Microbiology and Immunology, University of Melbourne, Peter Doherty Institute for Infection and Immunity, The University of Melbourne, Parkville, Victoria, Australia

[4]Department of Biochemistry and Molecular Biology, Bio21 Molecular Science and Biotechnology Institute, The University of Melbourne, Parkville, Victoria, Australia

[5]Molecular Signaling Section, Laboratory of Molecular Immunology, National Institute of Allergy and Infectious Diseases (NIAID), National Institutes of Health (NIH), Bethesda, Maryland, 20892, USA

[6]Centre for Personalised Immunology, The John Curtin School of Medical Research, Australian National University, Acton, Australian Capital Territory, Australia

[7]Department of Immunology, Canberra Hospital, Canberra, Australian Capital Territory, Australia

[8]Division of Chemistry and Structural Biology, Institute for Molecular Bioscience, The University of Queensland, Brisbane, Queensland, Australia

[9]ARC Centre of Excellence in Advanced Molecular Imaging, The University of Queensland, Brisbane, Queensland, Australia

[10]Department of Microbiology, Biomedicine Discovery Institute, Monash University, Clayton, Victoria, Australia

[*]Corresponding authors: Jamie Rossjohn jamie.rossjohn@monash.edu, Lauren J. Howson lauren.howson@monash.edu.
[†]These authors contributed equally to this work

Author contributions: Conceptualization L.J.H., M.S.D. and J.R.; Investigation L.J.H., W.A., A.v.B., H.J.L., H.E.G.M., M.L.S-R., S.M.; Formal Analysis A.R.H. and T.D.A.; Resources J.Y.W.M., L.L., D.P.F., J.M. and S.O.; Project administration L.J.H., D.H.M., P.M.M., J.L.N., J.A.V., M.C.C., S.O. and J.R.; Writing – Original Draft L.J.H. and J.R.; Supervision S.J.T., M.S.D. and J.R.

Competing interests: J.Y.W.M., L.L., D.P.F., J.M. and J.R. are inventors on patents describing MR1 tetramers and MR1 ligands.

Data and materials availability: The coordinates of the ternary complexes of MAIT A-F7 TCR-MR1^{R9H}-Ac-6-FP and TCR-MR1^{R9H}-empty have been deposited in the Protein Data Bank under accession codes: 6W9U and 6W9V. The whole exome sequencing data has been deposited in NCBI Sequence Read Archive.

[11]Department of Infectious Diseases, Monash Health, Clayton, Victoria, Australia

[12]Centre for Inflammatory Diseases, Monash University, Clayton, Victoria, Australia

[13]Institute of Infection and Immunity, Cardiff University School of Medicine, Heath Park, Cardiff, CF14 4XN, UK

Abstract

The role unconventional T cells play in protective immunity in humans is unclear. Mucosal-associated invariant T (MAIT) cells are an unconventional T cell subset restricted to the antigen presenting molecule MR1. Here, we report the discovery of a patient homozygous for a rare Arg31His (R9H) mutation in MR1 who has a history of difficult to treat viral and bacterial infections. $MR1^{R9H}$ was unable to present the potent microbially-derived MAIT cell stimulatory ligand. The $MR1^{R9H}$ crystal structure revealed that the stimulatory ligand cannot bind due to the mutation lying within, and causing structural perturbation to, the ligand binding domain of MR1. While $MR1^{R9H}$ could bind and be upregulated by a MAIT cell inhibitory ligand, the patient lacked circulating MAIT cells. This shows the importance of the stimulatory ligand for MAIT cell selection in humans. Interestingly, the patient had an expanded γδ T cell population, indicating a compensatory interplay between these unconventional T cell subsets.

Introduction

Unconventional T cells are a group of immune cell subsets that sit at the interface of innate and adaptive immunity. However, their role in coordinating and participating in human immune responses is unclear. This is partly due to the discrepancy in frequency and phenotype of these unconventional T cells between humans and mice (1). Mucosal-associated invariant T (MAIT) cells are a highly conserved unconventional T cell subset that is found in high frequency in humans (2, 3). These cells recognise microbially-derived vitamin B-related metabolites that are presented by the major histocompatibility complex class I-related molecule, MR1 (4, 5). Specifically, 5-(2-oxopropylideneamino)-6-D-ribitylaminouracil (5-OP-RU) is a very potent MAIT cell stimulatory ligand (6), while other ligands such as 6-formylpterin (6-FP), and its analogue acetyl-6-formylpterin (Ac-6-FP), can be presented by MR1 but do not activate MAIT cells (5).

Presently, mouse models of infection and observational studies in humans have largely shaped our understanding of the role MAIT cells play in immunity. MAIT cells have been identified and characterised in various disease settings, including bacterial infection in which they participate in TCR-dependent responses and play an important role in controlling the infection (7–10). They also participate in cytokine-mediated TCR-independent responses, where they play a role in controlling viral infection (11, 12) and have been implicated in autoimmunity (13) and cancer (14). In addition, a loss of MAIT cells (along with a loss of natural killer T (NKT) cells and interleukin (IL)-17A-producing T cells) has been reported in bi-allelic mutations in *RORC*. These individuals have difficulty controlling *Candida* and *Mycobacterium* infections, suggesting MAIT cells may be central in controlling these infections. However, examining the specific contribution of MAIT cells to human immunity

has not been explored and we do not know whether they are integral for protective immunity, or simply bystanders with a redundant role.

Here, we studied the role of MAIT cells in human immunity when an *MR1* mutation was identified in a patient with unexplained primary immunodeficiency, characterised by tattoo-associated persistent human papilloma virus $(HPV)^+$ warts. This patient is the first described case of a selective loss MAIT cells. We show that this lack of MAIT cells is due to an R9H mutation causing structural changes to the ligand-binding pocket of MR1, preventing the accommodation of the MAIT cell stimulatory ligand 5-OP-RU. Extensive immune phenotyping revealed an expanded $V\gamma9/V\delta2^+$ T cells, suggesting a potential immune compensatory mechanism by this innate T cell subset.

Results

Whole exome sequencing of a patient revealed a homozygous mutation MR1

A 31-year-old male patient was identified with unexplained primary immunodeficiency, characterised by tattoo-associated persistent human papilloma virus $(HPV)^+$ warts (Fig. S1). The patient also had a history of immune-related complications. Namely, treatment-refractory *Campylobacter* gastroenteritis when he was 25 years old, and development of pneumonia secondary to varicella-zoster virus infection that caused lung scarring when he was an infant (see supplementary text for full case report). The patient was selected for whole exome sequencing when the cause for this immunodeficiency could not be clinically determined. Whole exome sequencing revealed that the patient was homozygous for two rare single nucleotide variants (SNV) with immune-related functions (Fig. 1A, see Table S1 and S2 for full list of SNV).

The first SNV rs35337543, resulting in a splice variant of *IFIH1*, has been previously characterised as loss-of-function mutation of the MDA5 protein (15), and further examination of this gene mutation in the patient can be found in the rs35337543 SNV report (see Supplementary text and Fig. S2). Therefore, we focused on the patient's second homozygous immune-related SNV that is yet to be characterised, rs41268456 which is a G>A substitution at position 92 of the *MR1* transcript (c.92G>A). It occurs in an exon region that results in an arginine to histidine substitution at position 31 of the amino acid sequence, corresponding to position 9 of the mature MR1 protein after the signal peptide is cleaved (R9H) (Fig S3A). R9H has a combined annotation dependent depletion (CADD) score of 9.12, a polyphen score of 0.92 with a prediction of probably damaging. This mutation resides within the ligand-binding pocket of the MR1 amino acid sequence (Fig. 1B), with R9 being a conserved residue across mammalian species (Fig. S3B). Structural studies have shown that R9 lies within the A'-pocket of MR1 and interacts directly with the ligand, but this interaction differs depending on the ligand bound. For example, R9 forms hydrogen bonds with the ribityl 3'-hydroxyl group and the uracil C-2 carbonyl oxygen of 5-OP-RU (Fig. 1C), while making hydrogen bonds to the ring carbonyl oxygen of 6-FP (4, 5, 16). The patient was born to nonconsanguineous parents who were both heterozygous for the $MR1^{R9H}$ mutation, confirming an autosomal recessive inheritance pattern (Fig. 1B and D). The homozygous population frequency for rs41268456 is 0.000106 (15 individuals from a total cohort of 141 456), with a slightly higher frequency of 0.000203 in the European

population, based on the Genome Aggregation Database (gnomAD) cohort (17) (Fig. 1E). However, there is no clinical information available for the 15 homozygous individuals in the gnomAD database and there are yet to be any scientific studies that report the biological implications of this mutation.

The MR1$^{R9H/R9H}$ patient lacked circulating MAIT cells

To determine the functional implications of the *MR1*^{R9H} mutation, the frequency of MAIT cells in the peripheral blood of the *MR1*$^{R9H/R9H}$ patient was examined and compared to healthy age and gender matched donors with wild-type (WT) MR1 (Fig. S3C). The *MR1*$^{R9H/R9H}$ patient had no MAIT cells present based on MR1–5-OP-RU antigen-loaded tetramer staining or by staining with the MAIT cell surrogate markers: T cell receptor (TCR) Vα7.2 and CD161 (Fig. 2A). To confirm that the *MR1*$^{R9H/R9H}$ patient lacked functional MR1–5-OP-RU-reactive MAIT cells, we stimulated peripheral blood mononuclear cells (PBMC) with the MAIT cell antigen 5-OP-RU (6). In contrast to the response of PBMC from healthy controls, we failed to detect any circulating T cells producing TNF from the patient (Fig. 2B). We also confirmed that the Vα7.2^{+} CD161^{-} population did not display any difference compared to healthy donors in their reactivity to stimulation (Fig. S5). We next examined the circulating αβ T cell populations from the *MR1*$^{R9H/R9H}$ patient. He had a normal frequency of NKT cells but was mildly lymphopenic with reduced CD4 and CD8 T cell total cell counts and frequencies (Fig. S6A and Table S3). The *MR1*$^{R9H/R9H}$ T cells were also mostly comprised of memory T cells and showed a robust effector response to stimulation (Fig. S6B–C). Thus, the *MR1*$^{R9H/R9H}$ patient has a selective loss of MAIT cells, while all other T cell subsets remained intact.

The MR1$^{R9H/R9H}$ patient's antigen presenting cells were defective in antigen presentation

We next wanted to understand whether the lack of MAIT cells in the *MR1*$^{R9H/R9H}$ patient was a result of his antigen presenting cells being unable to present MAIT cell activating ligands. To test this, we pulsed B cells with 5-OP-RU and then cultured them with T cells from an allogenic *MR1*$^{WT/WT}$ donor. We found that *MR1*$^{R9H/R9H}$ B cells had a diminished capacity to activate the allogenic MAIT cells compared to B cells from a *MR1*$^{WT/WT}$ donor (Fig. 2C). Thus, the MR1^{R9H} mutation has a direct impact on MR1-restricted antigen presentation.

To directly examine the impact of the *MR1*^{R9H} mutation on ligand binding, we tested the capacity of *MR1*$^{R9H/R9H}$ B cells to upregulate MR1 in response to 5-OP-RU and the non-stimulatory MR1 ligand Ac-6-FP, both of which induce WT MR1 upregulation (18). We observed that, although the *MR1*$^{R9H/R9H}$ patient's B cells could upregulate MR1 upon addition of Ac-6-FP, 5-OP-RU did not induce MR1 upregulation (Fig. 3A). This observation was confirmed by examining MR1 upregulation on C1R cells overexpressing either MR1^{R9H} or WT MR1 (Fig. 3B and C). Thus, the *MR1*^{R9H} mutation appears to selectively disrupt 5-OP-RU binding to MR1.

The MR1^{R9H} mutation caused structural changes to the A'-pocket of MR1

To understand how the *MR1*^{R9H} mutation impacts ligand binding, we expressed and refolded MR1^{R9H} in the presence of Ac-6-FP and 5-OP-RU, then crystallised their co-

complexes with a MAIT cell TCR and subsequently solved the structures to high resolution (see Table S4 for all crystal structure supporting data). Surprisingly, MR1^{R9H} was refolded in the presence of 5-OP-RU but the A'-pocket was empty (Fig. 4A). WT MR1 requires binding of a ligand for stabilisation and correct folding (5). However, the MR1^{R9H} structure appears to not require the presence of a ligand to refold, similar to how the MR1^{K43A} mutant protein can be refolded without ligand (19). Indeed, MR1^{R9H} does refold in the absence of any exogenously added ligand (Fig. S7). Within the empty MR1^{R9H} A'-pocket, the imidazole side chain of the H9 residue formed new van der Waals interactions with the indole group of W69, causing W69 to flip and reorientate toward the base of the A'-pocket (Fig. 4A and Fig. S8B). In addition, water molecules found within the A'-pocket established a network of H-bonds with K43, H58, H9 and S24 residues. Together, these hydrophobic and polar interactions stabilised MR1^{R9H} enabling it to be refolded without ligand. Moreover, this reorientation of W69 and the presence of H9 partially fills the A'-pocket and sterically precludes 5-OP-RU binding (Fig. 4B). Interestingly however, MR1^{R9H} did refold and complex with Ac-6-FP, where the ligand formed a Schiff base with K43 of MR1 (Fig. 4C and S7D). Here, the reorientation of W69 does not interfere with Ac-6-FP binding, but forms hydrophobic interactions with the ligand in an analogous manner to how Ac-6-FP binds to WT MR1 (Fig. 4D). Consequently, while the non-stimulatory ligand can still bind MR1^{R9H}, the stimulatory ligand cannot.

The MR1^{R9H} mutation caused structural instability of MR1 impacting its cellular trafficking

Thermal stability assays showed that the empty MR1^{R9H} molecule was less stable compared to MR1^{R9H}-Ac-6-FP, and much less stable than WT MR1 when it is bound to either 5-OP-RU or Ac-6-FP (Fig. 5A). To examine whether the unstable nature of MR1^{R9H} impacted on its cellular trafficking, we examined its maturation through the secretory pathway by testing endoglycosidase H (endo-H) sensitivity. It has been previously shown that WT MR1 is largely retained in the endoplasmic reticulum (ER) (endo-H sensitive), and the presence of ligand causes it to refold and traffic through the Golgi apparatus to the cell surface (endo-H resistant) (18). We observed that MR1^{R9H} resides mostly in the ER, similar to WT MR1, and in the presence of Ac-6-FP it could traffic to the cell surface (Fig. 5B). Whereas upon addition of 5-OP-RU the MR1^{R9H} remained in the ER. Furthermore, when we examined the stability of MR1 molecules at the cell surface by measuring its rate of internalisation, MR1^{R9H} was internalised faster than WT MR1, both without ligand and in the presence of Ac-6-FP (Fig. 5C). These results confirm the MR1^{R9H} ligand discrimination that we have previously described above and also demonstrates the unstable nature of MR1^{R9H} at the cell surface.

The MR1$^{R9H/R9H}$ patient did not have any detectable MR1-restricted T cell populations

To examine the *MR1*$^{R9H/R9H}$ patient's MR1-restricted T cell populations, we stained PBMC with WT MR1 and MR1^{R9H} tetramers. The patient did not have any WT MR1-restricted T cell populations present (Fig. S9). We also did not observe any difference between *MR1*$^{WT/WT}$ controls' and *MR1*$^{R9H/R9H}$ patient's MR1^{R9H}-Ac-6-FP or -empty tetramer^{+} T cell frequencies, as no distinct populations were detected. This lack of TCR reactivity towards MR1^{R9H} was confirmed by surface plasmon resonance (SPR) experiments (Fig.

S10). Thus, the *MR1*$^{R9H/R9H}$ patient does not have any detectable MR1-restricted T cell populations.

Immune phenotyping of the MR1$^{R9H/R9H}$ patient's PBMC revealed that all other immune cell populations were present

We next wanted to determine whether the *MR1*$^{R9H/R9H}$ patient's immune system was altered or compensating for the absence of MAIT cells. Immune cell phenotyping revealed that the *MR1*$^{R9H/R9H}$ patient's circulating natural killer (NK) cell and monocyte frequencies were similar or slightly lower (for NK cells) compared to *MR1*$^{WT/WT}$ controls, and there were no major differences to the NK or monocyte subsets (Fig. S11). However, when examining the B cell subsets, we observed a reduction in memory B cells in the *MR1*$^{R9H/R9H}$ patient (Fig. S12). This lack of memory B cells could be an indication of deficient humoral immunity and is a typical observation made in a range of primary immunodeficiencies, such as: specific antibody deficiency and common variable immunodeficiency (20). However, the *MR1*$^{R9H/R9H}$ patient does still have detectable plasma cells (Fig. S12B), normal serum Ig levels (Table S5), and a robust vaccine response (see supplementary text) indicating that their low frequency of memory B cells does not have a considerable impact on the ability to mount humoral immune responses. These results confirm that the *MR1*$^{R9H/R9H}$ patient's immune cell subsets are otherwise intact, with only a possible impairment in their memory B cell compartment.

MR1$^{R9H/R9H}$ patient's Vγ9/Vδ2^{+} T cells were over-expanded and fully functional in response to various stimuli

We also examined the *MR1*$^{R9H/R9H}$ patient's γδ T cells and observed a 7-fold higher circulating frequency compared to healthy donors (Fig. 6A). This expanded γδ T cell population was almost exclusively comprised of Vγ9/Vδ2^{+} T cells (Fig. 6B) that had a distinct CD27^{-} CD28^{-} phenotype (Fig. 6C). This is not a hallmark of HPV infection associated with primary immunodeficiency, as we also analysed samples from patients with confirmed *CXCR4* gain-of-function mutations resulting in WHIM (warts, hypogammaglobulinemia, immunodeficiency, and myelokathexis) syndrome in which patients are highly susceptible to HPV infections (21, 22). The WHIM syndrome patients that tested HPV^{+} were examined and found to have a normal frequency of γδ T cells (Fig. 6A–B). We tested the functionality of the *MR1*$^{R9H/R9H}$ patient's Vγ9/Vδ2^{+} T cells and found that they exhibited intact effector functions in response to a range of different stimuli similar to *MR1*$^{WT/WT}$ controls (Fig. 6D). Paired TCR repertoire analysis revealed that the *MR1*$^{R9H/R9H}$ patient's Vγ9/Vδ2^{+} T cells are clonally expanded, with one dominant clone comprising ~30% of the γδ T cell population (Fig. 6E), which is not typically seen in Vγ9/Vδ2^{+} T cells from healthy donors (23). An unusual feature of the *MR1*$^{R9H/R9H}$ patient's Vγ9/Vδ2^{+} T cell population was that 50% of the TCR repertoire used the *TRDJ3* gene segment, compared to healthy adults which predominantly use *TRDJ1* (Fig. 6F).

Next we examined the total TNF/IFNγ production by PBMC in response to stimuli. The *MR1*$^{R9H/R9H}$ PBMC showed a robust TNF/IFNγ response, for which 89% of the cells producing cytokine in response to *E. coli* were the Vγ9/Vδ2^{+} T cells (Fig. 7A). To confirm this robust antibacterial response, we challenged PBMC *ex vivo* to a variety of bacteria

and examined the total cytokine production and cytotoxic response. We found that the patient's PBMC could produce proinflammatory cytokines and cytotoxic granules to all bacteria strains to the same extent as healthy donors (Fig. 7B and Fig. S13). These results suggest that the *MR1*$^{R9H/R9H}$ patient is still able to produce a robust effector response when challenged with bacteria.

Discussion

The discovery of a patient with a homozygous mutation that impacts MR1 presentation provided a unique opportunity to understand the role and importance of MAIT cells in human immunity. Alterations in MAIT cells has been observed in primary immunodeficiencies previously, where they are decreased in individuals with dominant mutations in *STAT3* (24) and recessive mutations in *IL12RB1* or *IL23R* (25). Furthermore, MAIT cells (along with NKT cells and IL-17A producing T cells) are absent in cases of bi-allelic mutations in *RORC* (26). However, the immune phenotype of the *MR1*$^{R9H/R9H}$ patient is distinct, as there is a selective absence of MAIT cells.

Our observation that the *MR1*^{R9H} homozygous mutation leads to in a lack of MAIT cells provides some insight into what factors are vital for MAIT cell selection and/or survival in humans. As MR1^{R9H} cannot present 5-OP-RU, is suggests that 5-OP-RU itself, or ligands that are structurally similar to 5-OP-RU, are required for the selection and survival of MAIT cells in humans, consistent with a study that recently demonstrated this concept in mice (27).

A striking observation was the expansion of Vγ9/Vδ2$^+$ T cells observed in the *MR1*$^{R9H/R9H}$ patient. This observation is consistent with the observed $\gamma\delta$ T cell expansion reported in *RORC* mutated individuals (that lack MAIT cells) (26), suggesting this could be an immune compensatory mechanism that occurs when MAIT cells are not present. This is unexpected, as it has been previously hypothesised that NKT cells, which are the most functionally and transcriptionally similar to MAIT cells (28), were the most likely cell subset to share a functional niche with MAIT cells. This was further supported by the observation that MAIT cells are expanded in CD1d knockout mice that lack NKT cells (29). Further evidence that Vγ9/Vδ2$^+$ T cells and MAIT cells reside in the same functional niche is the *MR1*$^{R9H/R9H}$ patient's robust *ex vivo* anti-bacterial immune response which is largely mediated by the expanded Vγ9/Vδ2$^+$ T cells. This observed *ex vivo* immune compensation may explain why the MR1$^{R9H/R9H}$ patient does not have a history of more severe and frequent bacterial infections, even though they lack MAIT cells.

Another unusual observation was the enrichment of the *TRDJ3* TCR gene segment usage by Vγ9/Vδ2$^+$ T cells. Enrichment of this gene segment is a hallmark of Vγ9/Vδ2$^+$ T cells that are generated during ontogeny in the fetal thymus, compared to adult Vγ9/Vδ2$^+$ T cells that typically use *TRDJ1* and are generated independently of the thymus after birth (30). Thus, the Vγ9/Vδ2$^+$ T cell population may have undergone selective pressures during early development of the *MR1*$^{R9H/R9H}$ patient's immune system and resulted in retention and expansion of "fetal-like" Vγ9/Vδ2$^+$ T cells.

The clinical aspect of this patient's case is the onset of persistent HPV$^+$ warts associated with extensive tattooing. Difficult to treat HPV is a hallmark of primary immunodeficiency, although the mechanism is unclear as the host immune defence against HPV is multifaceted, with immunity provided from various immune cells as well as non-immune cells such as keratinocytes (31, 32). There have also been several cases reported of tattoo-associated HPV in otherwise immunocompetent individuals (33, 34), but in these cases the lesions are localised to the tattoo itself, unlike the patient who has widespread lesions. This suggests that the barrier disruption caused by tattooing may contribute to the host's lack of ability to mount an effective immune response against HPV. However, without information about which immune cells are at the site of the HPV lesions it is not known which cells are implicated in the patient's HPV-specific immune response.

A limitation of this study is that as we have identified and characterised the *MR1*^{R9H} mutation in a single patient with two identified immune-related homozygous mutations in *MR1* and *IFIH1*. This makes it difficult to attribute a clinical phenotype to the lack of MAIT cells caused by the *MR1* mutation. Thus, a greater understanding would be gained from studying this mutation across multiple homozygous and heterozygous individuals to appreciate the nature and penetrance of clinical symptoms associated with *MR1*^{R9H} and degree of microbial susceptibility in those with who carry this mutation.

Materials and Methods

Study Design

The *MR1*$^{R9H/R9H}$ patient was recruited to the Genetic Immunology Flagship of Australian Genomics Health Alliance, which was approved by human research ethics committees at ACT Health Human Research Ethics Committee and Melbourne Health (protocols ETH.8.17.171E and HREC/16/MH/251) for whole exome sequencing to determine the underlying cause of his primary immunodeficiency. Immune phenotyping of the patient's blood samples was done with ethical approval for additional samples collected on three separate occasions at Monash Medical Centre from the Monash Health Human Research Ethics Committee (project ID: 52046). The *MR1*$^{R9H/R9H}$ patient's parents' blood was also collected for immune phenotyping. For comparison to the patient, age- and gender-matched healthy donors were recruited and blood samples taken with ethical approval from the Monash University Human Research Ethics Committee (project ID: 19488). To provide a HPV$^+$ control group for immune phenotyping comparison, WHIM patient samples were collected as part of a clinical research protocol approved by the Institutional Review Board of the National Institute of Allergy and Infectious Diseases, NIH. Written informed consent was obtained for all study volunteers in accordance with the Declaration of Helsinki. The study was unblinded and sample sizes were limited by the availability of donors but adequate to detect differences between sample groups.

Whole exome sequencing

Genomic DNA was isolated from blood using the QIAamp DNA Blood Kit (Qiagen) according to the manufacturer's instructions. For whole exome sequencing, Input DNA was analysed for integrity then fragmented by nebulization. DNA library preparation was

performed using Agilent High Sensitivity whole exome capture and libraries were sequenced as paired end reads (100 bp runs) on an Illumina HiSeq 2500. Bioinformatics analysis was performed as previously described (35).

Human samples

Patients were recruited to the study at the Monash Medical Centre and a blood sample taken during a routine appointment. Healthy adult blood donors were from laboratory volunteers, from buffy packs obtained from Australian Red Cross Lifeblood or were obtained from the National Institutes of Health (NIH) Clinical Center Department of Transfusion Medicine. Peripheral blood mononuclear cells (PBMC) were isolated from all blood samples and buffy packs by gradient centrifugation using Lymphoprep™ (STEMCELL Technologies) or Ficoll-Paque PLUS density gradient media (GE Healthcare). Cells were then either used fresh or cryogenically frozen for later analysis.

Polymerase chain reaction (PCR) confirmation of IFIH1 splice variation

RNA was extracted from PBMC samples using the PureLink™ RNA Mini Kit (Ambion) and cDNA produced using SuperScript™ IV First-Strand Synthesis System (Invitrogen™) following the manufacturer's instructions. The cDNA was then used in a standard PCR reaction with GoTaq® Green Master Mix (Promega) following manufacturer's instructions using the following primers designed to amplify the regions flanking exon 8 of the *IFIH1* transcript: IFIH1.F, 5'-ACGAAGCAAGCCAAAGCTGA and IFIH1.R 5'-GGCCCATTGTTCATAGGGTTGA. Samples were then run on a 2% agarose gel with a 100 bp DNA ladder (New England Biolabs). Band size of the PCR product indicated whether the exon 8 was present (258 bp) or absent (139 bp).

TaqMan® qPCR assay for IFNA1 and IFNB1 induction

PBMC were cultured with or without 10 μg/mL Poly(I:C) high molecular weight (HMW)/LyoVec™ (InvivoGen) for 24 hr. RNA was extracted and cDNA synthesised as described in the previous section. The cDNA was then used in a TaqMan® qPCR assay using TaqMan™ Fast Advanced Master Mix (Applied Biosystems) with TaqMan® Gene Expression Assays for *IFNA1* and *IFNB1* and the reference gene *HPRT1* (Thermo Fisher Scientific). Samples were then run on a CFX Connect Real-Time PCR Detection System (Bio-Rad) and quantified using the Comparative CT Method ($2^{-\Delta\Delta CT}$ method).

Sanger sequencing of MR1

RNA was extracted and cDNA synthesised as described in the previous section. The cDNA was then used in a standard PCR reaction with GoTaq® Green Master Mix following manufacturer's instructions using the following primers designed to amplify position R9 on the *MR1* transcript: MR1.F, 5'-GGAACTGATGGCGTTCCTGT and MR1.R, 5'-GTGGTGATAGGGTGCGAGTC. Samples were then sequenced with BigDye Terminator v3.1 (Applied Biosystems) following manufacturer's instructions and run on an Applied Biosystems 3730S capillary sequencer (Micromon Genomics, Monash University). Results were visualised using SnapGene® Viewer.

Antibodies and staining reagents

APC anti-human CD56 (NCAM16.2), BB700 anti-human CD19 (SJ25C1), BUV395 anti-human CD3 (NCAM16.2), BUV395 anti-human CD8 (RPA-T8), BV786 anti-human IFN-γ (4S.B3), FITC anti-human IgM (G20–127), PE Streptavidin, PE-CF594 anti-human IgD (IA6–2) and PerCP-Cy™5.5 anti-human TNF (MAb11) were purchased from BD Biosciences. Alexa Fluor® 700 anti-human CD16 (3G8), Alexa Fluor® 700 anti-human CD4 (SK3), APC or Alexa Fluor® 700 anti-human CD161 (HP-3G10), Brilliant Violet 605™ anti-human CD38 (HIT2), Brilliant Violet 605™ anti-human TCR Vα7.2 (3C10), Brilliant Violet 650™ anti-human CD28 (CD28.2), Brilliant Violet 711™ anti-human CD45RA (HI100), Brilliant Violet 785™ anti-human CD45RO (UCHL1), PE anti-human CD14 (M5E2), PE anti-human IL-2 (MQ1–17H12), PE/Cy7 anti-human CD27 (M-T271), PE/Cy7 anti-human CD3 (UCHT-1) and PE/Dazzle 594 anti-human CD27 (M-T271) were purchased from Biolegend. APC anti-human TCR Vδ2 (123R3), APC-Vio770 anti-human TCRγ/δ (REA591), FITC anti-human TCR Vδ1 (REA173) and VioBlue anti-human TCRα/β (REA652) were purchased from Miltenyi Biotec. PC5 anti-human TCR Vγ9 (IMMU 360) was purchased from Beckman Coulter. A hybridoma cell line was used to produce the MR1 8F2.F9 and 26.5 antibodies (36). PBS-57-loaded CD1d tetramer was obtained from the NIH tetramer core facility. Dead cells were excluded using the viability dye LIVE/DEAD® Fixable Aqua Dead Cell Stain Kit (Life Technologies). For immunoprecipitation experiments, a polyclonal rabbit antiserum was generated by the Walter and Eliza Hall Institute Antibody Facility against a peptide corresponding to the final 15 residues of the cytosolic tail of human MR1 (PREQNGAIYLPTPDR) (anti-MR1-CT).

Flow cytometry and cell sorting

For standard flow cytometry cell staining, cells were first stained with viability dye for 10 min at room temperature, followed by antibodies diluted in phosphate buffered saline with 10% foetal bovine serum (Sigma) for 20 min on ice. Flow cytometry data was collected on a BD LSRFortessa™ X20. Cell sorting was performed on BD FACSAria™ Fusion Cell Sorter. Data was analysed using FlowJo™ cell analysis software (FlowJo, LLC).

Ligands and compounds

Production of 5-OP-RU has been described previously (6). Ac-6-FP was purchased from Schircks Laboratories.

Mucosal-associated invariant T (MAIT) cell activation assay

PBMC were cultured with 1 nM 5-OP-RU for 4 hr, then Brefeldin A solution (eBioscience) was added and cells cultured for 18 hr. Cells were collected and stained with viability dye, prior to fixation and permeabilisation using the eBioscience™ Intracellular Fixation & Permeabilisation Buffer Set (Invitrogen). Antibodies diluted in permeabilisation buffer were then incubated with cells for 45 min at room temperature.

Cell lines

Production of C1R cells overexpressing MR1 under the control of the p-MSCV-IRES-eGFP (pMIG) vector have been previously described (37). Using this protocol we produced C1R

cells expressing a single amino acid substitution R9H in MR1 by designing gBlock gene fragments (IDT) and cloning it into the pMIG vector and transfecting it into 293T cells with the retroviral packaging vectors (pPAM-E and pVSVG) using Fugene 6. The supernatant containing viral particles was then filtered through a 0.45 μm filter and added to WT C1R cells with polybrene to produce a stable transduction of cells overexpressing $MR1^{R9H}$. The transduced C1R.$MR1^{R9H}$ cell line was then sorted for high expression of GFP and MR1.

Bacterial cultures

The bacteria: *Escherichia coli*, *Pseudomonas aeruginosa*, *Staphylococcus aureus, Staphylococcus epidermidis* and *Enterococcus faecalis* were grown in Lysogeny broth (LB) overnight, then diluted 1:100 and grown to log phase for 3 hr. OD_{600} was measured and used to determine concentration.

MR1 upregulation assay

Cells were cultured in the presence of 5-OP-RU (1 μM) or Ac-6-FP (10 μM) for 4 hr (unless specified otherwise) prior to staining with viability dye. Cells were then stained with biotinylated MR1 8F2.F9 for 30 min on ice, followed by streptavidin-PE (and any directly conjugated primary antibodies, if being used) for 20 min on ice. Cells were then analysed on a flow cytometer.

Expression, Refold and Purification of MR1-β2m and MAIT TCR proteins

Human WT MR1-β2m and $MR1^{R9H}$-β2m were refolded in the presence of either Ac-6-FP or 5-OP-RU, as described previously (4). Human $MR1^{R9H}$-β2m-empty was refolded in the absence of any ligand, producing refolded protein, confirmed by native gel and size exclusion chromatography (Fig, S6). Soluble A-F7 (TRAV1–2/TRBV6–1) and TRAV1–2/TRBV6–4 MAIT TCR proteins were refolded from inclusion bodies, as described previously (38, 39). Refolded MR1-ligand and TCR proteins were purified by three consecutive purification steps: crude anion exchange, S200 15/60 size exclusion chromatography and HiTrap-Q HP anion exchange. The protein purity was then assessed using sodium dodecyl sulfate–polyacrylamide gel electrophoresis (SDS-PAGE) and quantified using a NanoDrop™ spectrophotometer.

Generation of MR1 tetramers

C-terminal cysteine-tagged human-MR1-β2m (complexed with ligand where indicated) were refolded and purified, as described in the previous section. The purified proteins were reduced by dithiothreitol (DTT), buffer exchanged into HEPES buffered saline (10 mM HEPES pH 7.3, 150 mM NaCl, 1 mM EDTA), and then biotinylated by incubation with biotin-maleimide overnight at 4°C. The biotinylated samples were purified by gel filtration and biotinylation efficiency was assessed by native gel. Biotinylated proteins were then tetramerised with PE-conjugated streptavidin and used to stain cells at a 1:50 dilution.

Thermal stability assay

A thermal shift assay of the WT MR1 and $MR1^{R9H}$ proteins was performed in a real-time detection system (Corbett RotorGene 3000) using the fluorescent dye SYPRO® Orange

(Sigma) to monitor the protein unfolding upon heating. Both WT and MR1^{R9H} (complexed with ligand where indicated) were purified by gel filtration just before the experiment and eluted in buffer of 10 mM Tris-HCl (pH 8), 150 mM NaCl. The samples were then heated from 25–95℃ with a heating rate of 1℃/min. The fluorescence intensity was measured (excitation 530 nm, emission 610 nm) and used to infer protein unfolding. The half maximum melting point (Tm50) represents the temperature for which 50% of the protein is unfolded.

Protein Crystallization, Structure Determination and Refinement

Purified TRAV1–2-TRBV6–1 TCR was mixed with either WT or MR1^{R9H} proteins (complexed with ligand where indicated) in 1:1 molar ratio at concentration of 2–4 mg/mL and incubated on ice for 4 hr. Hanging-drop method was employed to produce crystals with a precipitant consisting of 100 mM BTP (pH 6.1–6.7), 8–14% PEG3350 and 200 mM sodium acetate, as reported previously (38). Hexagonal complex crystals formed within a week at 20℃ and were flash frozen in liquid nitrogen after a short soak in reservoir solution with 14% glycerol and 10× molar amount of the loaded ligand (either 5-OP-RU or Ac-6-FP) for cryo-protection. X-ray diffraction data was collected at 100 K on the Australian Synchrotron at either MX1 or MX2 beamlines. Diffraction images were processed using XDS (40) and programs from the CCP4 suite (41) and Phenix package (42). Both ternary structures were determined by molecular replacement using PHASER (43), where modified TCR-MR1 ternary complex (PDB: 4NQC) was used as a search model. Model building was performed in COOT (44), accompanied with iterative rounds of refinement using Phenix.refine (42). The Grade Webserver and Phenix tools were used to build and to generate ligand restraints. The models were validated using MolProbity (45) and graphical representations were generated using PyMOL Molecular Graphics System, Version 1.8 (Schrödinger, LLC, New York, NY).

Immunoprecipitation

For immunoblotting and detection of MR1, cells were lysed in 0.5% IGEPAL CA-630 (Sigma-Aldrich), 50 mM Tris-HCl (pH 7.4), 5 mM $MgCl_2$ with Complete Protease Inhibitor Cocktail (Roche), and nuclei separated by centrifugation at 13,000 × *g* for 10 min. Lysates were precleared with normal rabbit serum (Sigma-Aldrich) and protein G-Sepharose then with protein G-Sepharose alone. MR1 was immunoprecipitated using anti-MR1-CT and protein G-Sepharose, and then washed three times with NET buffer (0.5% IGEPAL CA-630, 50 mM Tris-Cl pH 7.4, 150 mM NaCl, 5 mM EDTA) and treated with Endoglycosidase Hf (New England Biolabs) according to the manufacturer's instructions. Protein samples were denatured with reducing SDS-PAGE sample buffer, separated on NuPAGE 4–12% Bis-Tris precast gel (Life Technologies) and immunoblotted onto nitrocellulose membrane using the iBlot system (Life Technologies). Band density was quantified using FIJI analysis software.

Internalisation assay

To measure MR1 internalisation, a fluorescence internalisation probe (FIP) using 8F2.F9 MR1 antibody was generated as previously described (46). Briefly, the FIP conjugated to MR1 contains a DNA sequence conjugated to the fluorescent dye Cy5, which can be quenched by using a quencher conjugated to the complementary DNA sequence. Any Cy5

signal not quenched indicates protection due to internalisation. Cells were labelled with MR1-FIP on ice, then washed and incubated at 37°C for the indicated times prior to being placed on ice to halt internalisation. Cells were washed and resuspended with or without the quencher, and Cy5 fluorescence analysed by flow cytometry. The Cy5 signal remaining after quenching indicates internalised MR1 and was calculated as a percentage of the initial signal before internalisation.

γδ T cell activation assay

PBMC were cultured and pulsed with a range of stimulants. For cytokine stimulation: 100 U/mL human interleukin (IL)-2 (Roche), 200 ng/mL human IL-12 (Miltenyi Biotec) and 200 ng/mL human IL-18 (Biolegend), two doses 72 hr apart, with brefeldin A (BFA) (Biolegend) added after second dose and cultured for 18 hr. For bacterial stimulation: *E. coli* at multiplicity of infection (MOI) 50 was added to PBMC, left for 1 hr prior to adding 50 μg/mL gentamicin (Sigma) and BFA and cultured for 18 hr. For (E)-4-Hydroxy-3-methyl-but-2-enyl pyrophosphate (HMBPP) stimulation: 10 ng/mL of HMBPP (Cayman Chemicals) was added and cultured for 4 hr before adding BFA and cultured for 18 hr. For a positive control: 50 ng/mL phorbol 12-myristate 13-acetate (PMA) (Sigma) and 1 μg/mL ionomycin (Sigma) were added with BFA and cultured for 18 hr. Following stimulation, cells were collected and stained with viability dye and stained with surface antibodies for 20 min on ice, prior to fixation and permeabilisation using the eBioscience™ Intracellular Fixation & Permeabilisation Buffer Set (Invitrogen). Intracellular antibodies were then incubated for 45 min diluted in permeabilisation buffer.

Single cell γδ TCR sequencing

PBMC were surface stained with antibodies and γδ T cells were single cell sorted directly into individual wells in a 96-well PCR plate containing 2 μL of SensiFAST cDNA Synthesis Kit reaction mix (Bioline) with 0.1% Triton X-100. Samples were incubated according to manufacturer's instructions. TCRγ and TCRδ sequences were amplified using two rounds of nested PCR using GoTaq mastermix (Promega) and primers for Vδ2: TCTGGGCAGGAGTCATGT (external) and GAAAGGAGAAGCGATCGGTAAC (internal); Cδ: GCAGGATCAAACTCTGTTATCTTC (external) and TCCTTCACCAGACAAGCGAC (internal); Vγ1–8: CTGGTACCTACACCAGGAGGGGAAGG (external) and TGTGTTGGAATCAGGAVTCAG (internal); Vγ9: AGAGAGACCTGGTGAAGTCATACA (external) and GGTGGATAGGATACCTGAAACG (internal); and Cγ: CTGACGATACATCTGTGTTCTTTG (external) and AATCGTGTTGCTCTTCTTTTCTT (internal). PCR products were visualized on a 2% agarose gel, and products of successful reactions were incubated ExoSAP-IT™ PCR Product Cleanup Reagent (Applied Biosystems) before sequencing with BigDye Terminator v3.1 (Applied Biosystems) following the manufacturer's instructions and running on an Applied Biosystems 3730S capillary sequencer (Micromon Genomics, Monash University). Results were visualised using SnapGene® Viewer.

Bulk γδ TCR repertoire sequencing

RNA was purified from 10 000 sorted $V\gamma9^{+}V\delta2^{+}$ T cells using an RNAmicro kit (Qiagen) according to the manufacturer's instructions. Amplicon rescued multiplex-PCR and next generation sequencing (NGS) methods (47) were used to analyse the sorted γδ T cell population from three healthy donors. Following initial first-round reverse transcription PCR using high concentrations of gene-specific primers, universal primers were used for the exponential phase of amplification (48). (Patent: WO2009137255A2). All cDNA synthesis, amplification, NGS library preparation were performed using the TRD/TRG iR-profile kits (HTGI-M or HTDI-M; iRepertoire, Inc. Huntsville, USA) and subsequent libraries were pooled and deep sequenced using an illumina MiSeq NGS platform (Micromon Genomics, Monash University).

Allogenic T cell/B cell coculture assay

B cells were isolated from PBMC using B Cell Isolation Kit II, human (Miltenyi Biotec) and T cells from an allogenic donor were isolated using CD2 MicroBeads, human (Miltenyi Biotec) and cell isolation was performed using the Miltenyi Biotec MidiMACS™ separator following the manufacturer's instructions. B cells were cultured with 5-OP-RU at indicated concentrations for 4 hr. The B cells were then washed twice prior to addition of BFA and allogenic (MHC miss-matched, as MR1 is monomorphic) T cells at 1:1 effector:target ratio and cultured for 18 hr. Cells were collected and stained with viability dye, prior to fixation and permeabilisation using the eBioscience™ Intracellular Fixation & Permeabilisation Buffer Set (Invitrogen). Antibodies diluted in permeabilisation buffer were then incubated for 45 min at room temperature.

Whole PBMC ex vivo bacterial challenge

PBMC were cultured with the indicated bacteria at MOI 50 for 1 hr, then 50 μg/mL gentamicin was added and cultured for 24 hr. Supernatant was then collected and the cytokine and cytotoxic profile examined using the LEGENDplex™ CD8/Natural Killer (NK) panel following the manufacturer's instructions. Samples were then run on a BD LSRFortessa™ X20 and data analysed using the LEGENDplex™ Data Analysis Software.

Statistical Analysis

Statistical analysis was performed using GraphPad Prism version 8 for macOS, GraphPad Software, San Diego, California USA. For multiple comparisons with two independent variables two-way ANOVA with Geisser-Greenhouse correction and Sidak's multiple comparison test was used. Significant result is indicated where $P < 0.05$.

Supplementary Material

Refer to Web version on PubMed Central for supplementary material.

Acknowledgments:

We would like to thank all study participants; A. Fletcher (Monash University) and D. Velez (NIH) for assistance with healthy donor blood collection; F. Morris and A. Peleg (Monash University) for providing bacterial strains and S. Tangye (Garvin Institute of Medical Research) for critical reading of the manuscript. We acknowledge use of the

services and facilities of Micromon Genomics at Monash University and FlowCore for sorting of cells using FACS. This research was undertaken in part by using the MX2 beamline at the Australian Synchrotron, part of ANSTO, and made use of the Australian Cancer Research Foundation (ACRF) detector.

Funding:

This work was supported by a program grant from the National Health and Medical Research Council of Australia (NHMRC) (1013667 & 1016629), a Targeted Call for Research grant (NHMRC) (1113531), the Australian Research Council (ARC) (CE140100011) and the Division of Intramural Research, NIAID/NIH. J.L.N. is supported by an ARC Future Fellowship (FT160100074); D.P.F. is supported by NHMRC Senior Principal Research Fellowship (1117766); M.S.D. is supported by an ARC DECRA Fellowship; J.R. is supported by an Australian ARC Laureate Fellowship.

References and Notes:

1. Godfrey DI, Uldrich AP, McCluskey J, Rossjohn J, Moody DB, The burgeoning family of unconventional T cells. Nat Immunol 16, 1114–1123 (2015). [PubMed: 26482978]
2. Dusseaux M, Martin E, Serriari N, Peguillet I, Premel V, Louis D, Milder M, Le Bourhis L, Soudais C, Treiner E, Lantz O, Human MAIT cells are xenobiotic-resistant, tissue-targeted, CD161hi IL-17-secreting T cells. Blood 117, 1250–1259 (2011). [PubMed: 21084709]
3. Walker LJ, Tharmalingam H, Klenerman P, The Rise and Fall of MAIT Cells with Age. Scand J Immunol 80, 462–463 (2014). [PubMed: 25196940]
4. Corbett AJ, Eckle SB, Birkinshaw RW, Liu L, Patel O, Mahony J, Chen Z, Reantragoon R, Meehan B, Cao H, Williamson NA, Strugnell RA, Van Sinderen D, Mak JY, Fairlie DP, Kjer-Nielsen L, Rossjohn J, McCluskey J, T-cell activation by transitory neo-antigens derived from distinct microbial pathways. Nature 509, 361–365 (2014). [PubMed: 24695216]
5. Kjer-Nielsen L, Patel O, Corbett AJ, Le Nours J, Meehan B, Liu L, Bhati M, Chen Z, Kostenko L, Reantragoon R, Williamson NA, Purcell AW, Dudek NL, McConville MJ, O'Hair RA, Khairallah GN, Godfrey DI, Fairlie DP, Rossjohn J, McCluskey J, MR1 presents microbial vitamin B metabolites to MAIT cells. Nature 491, 717–723 (2012). [PubMed: 23051753]
6. Mak JY, Xu W, Reid RC, Corbett AJ, Meehan BS, Wang H, Chen Z, Rossjohn J, McCluskey J, Liu L, Fairlie DP, Stabilizing short-lived Schiff base derivatives of 5-aminouracils that activate mucosal-associated invariant T cells. Nat Commun 8, 14599 (2017). [PubMed: 28272391]
7. Howson LJ, Napolitani G, Shepherd D, Ghadbane H, Kurupati P, Preciado-Llanes L, Rei M, Dobinson HC, Gibani MM, Teng KWW, Newell EW, Veerapen N, Besra GS, Pollard AJ, Cerundolo V, MAIT cell clonal expansion and TCR repertoire shaping in human volunteers challenged with Salmonella Paratyphi A. Nat Commun 9, 253 (2018). [PubMed: 29343684]
8. Meierovics A, Yankelevich WJC, Cowley SC, MAIT cells are critical for optimal mucosal immune responses during in vivo pulmonary bacterial infection. P Natl Acad Sci USA 110, E3119–E3128 (2013).
9. Georgel P, Radosavljevic M, Macquin C, Bahram S, The non-conventional MHC class I MR1 molecule controls infection by Klebsiella pneumoniae in mice. Mol Immunol 48, 769–775 (2011). [PubMed: 21190736]
10. Chen Z, Wang H, D'Souza C, Sun S, Kostenko L, Eckle SB, Meehan BS, Jackson DC, Strugnell RA, Cao H, Wang N, Fairlie DP, Liu L, Godfrey DI, Rossjohn J, McCluskey J, Corbett AJ, Mucosal-associated invariant T-cell activation and accumulation after in vivo infection depends on microbial riboflavin synthesis and co-stimulatory signals. Mucosal Immunol 10, 58–68 (2017). [PubMed: 27143301]
11. van Wilgenburg B, Scherwitzl I, Hutchinson EC, Leng TQ, Kurioka A, Kulicke C, de Lara C, Cole S, Vasanawathana S, Limpitikul W, Malasit P, Young DC, Denney L, Moore MD, Fabris P, Giordani MT, Oo YH, Laidlaw SM, Dustin LB, Ho LP, Thompson FM, Ramamurthy N, Mongkolsapaya J, Willberg CB, Screaton GR, Klenerman P, Consortium S-H, MAIT cells are activated during human viral infections. Nat Commun 7, 11653 (2016). [PubMed: 27337592]
12. van Wilgenburg B, Loh L, Chen Z, Pediongco TJ, Wang H, Shi M, Zhao Z, Koutsakos M, Nussing S, Sant S, Wang Z, D'Souza C, Jia X, Almeida CF, Kostenko L, Eckle SBG, Meehan BS, Kallies A, Godfrey DI, Reading PC, Corbett AJ, McCluskey J, Klenerman P, Kedzierska K, Hinks TSC,

MAIT cells contribute to protection against lethal influenza infection in vivo. Nat Commun 9, 4706 (2018). [PubMed: 30413689]

13. Willing A, Leach OA, Ufer F, Attfield KE, Steinbach K, Kursawe N, Piedavent M, Friese MA, CD8(+) MAIT cells infiltrate into the CNS and alterations in their blood frequencies correlate with IL-18 serum levels in multiple sclerosis. Eur J Immunol 44, 3119–3128 (2014). [PubMed: 25043505]
14. Ling LM, Lin YY, Zheng WW, Hong S, Tang XQ, Zhao PW, Li M, Ni JS, Li CG, Wang L, Jiang YF, Circulating and tumor-infiltrating mucosal associated invariant T (MAIT) cells in colorectal cancer patients. Sci Rep 6, 20358 (2016). [PubMed: 26837580]
15. Asgari S, Schlapbach LJ, Anchisi S, Hammer C, Bartha I, Junier T, Mottet-Osman G, Posfay-Barbe KM, Longchamp D, Stocker M, Cordey S, Kaiser L, Riedel T, Kenna T, Long D, Schibler A, Telenti A, Tapparel C, McLaren PJ, Garcin D, Fellay J, Severe viral respiratory infections in children with IFIH1 loss-of-function mutations. Proc Natl Acad Sci U S A 114, 8342–8347 (2017). [PubMed: 28716935]
16. Awad W, Ler GJM, Xu W, Keller AN, Mak JYW, Lim XY, Liu L, Eckle SBG, Le Nours J, McCluskey J, Corbett AJ, Fairlie DP, Rossjohn J, The molecular basis underpinning the potency and specificity of MAIT cell antigens. Nat Immunol 21, 400–411 (2020). [PubMed: 32123373]
17. Karczewski KJ, Francioli LC, Tiao G, Cummings BB, Alföldi J, Wang Q, Collins RL, Laricchia KM, Ganna A, Birnbaum DP, Gauthier LD, Brand H, Solomonson M, Watts NA, Rhodes D, Singer-Berk M, England EM, Seaby EG, Kosmicki JA, Walters RK, Tashman K, Farjoun Y, Banks E, Poterba T, Wang A, Seed C, Whiffin N, Chong JX, Samocha KE, Pierce-Hoffman E, Zappala Z, O'Donnell-Luria AH, Minikel EV, Weisburd B, Lek M, Ware JS, Vittal C, Armean IM, Bergelson L, Cibulskis K, Connolly KM, Covarrubias M, Donnelly S, Ferriera S, Gabriel S, Gentry J, Gupta N, Jeandet T, Kaplan D, Llanwarne C, Munshi R, Novod S, Petrillo N, Roazen D, Ruano-Rubio V, Saltzman A, Schleicher M, Soto J, Tibbetts K, Tolonen C, Wade G, Talkowski ME, Aguilar Salinas CA, Ahmad T, Albert CM, Ardissino D, Atzmon G, Barnard J, Beaugerie L, Benjamin EJ, Boehnke M, Bonnycastle LL, Bottinger EP, Bowden DW, Bown MJ, Chambers JC, Chan JC, Chasman D, Cho J, Chung MK, Cohen B, Correa A, Dabelea D, Daly MJ, Darbar D, Duggirala R, Dupuis J, Ellinor PT, Elosua R, Erdmann J, Esko T, Färkkilä M, Florez J, Franke A, Getz G, Glaser B, Glatt SJ, Goldstein D, Gonzalez C, Groop L, Haiman C, Hanis C, Harms M, Hiltunen M, Holi MM, Hultman CM, Kallela M, Kaprio J, Kathiresan S, Kim B-J, Kim YJ, Kirov G, Kooner J, Koskinen S, Krumholz HM, Kugathasan S, Kwak SH, Laakso M, Lehtimäki T, Loos RJF, Lubitz SA, Ma RCW, MacArthur DG, Marrugat J, Mattila KM, McCarroll S, McCarthy MI, McGovern D, McPherson R, Meigs JB, Melander O, Metspalu A, Neale BM, Nilsson PM, O'Donovan MC, Ongur D, Orozco L, Owen MJ, Palmer CNA, Palotie A, Park KS, Pato C, Pulver AE, Rahman N, Remes AM, Rioux JD, Ripatti S, Roden DM, Saleheen D, Salomaa V, Samani NJ, Scharf J, Schunkert H, Shoemaker MB, Sklar P, Soininen H, Sokol H, Spector T, Sullivan PF, Suvisaari J, Tai ES, Teo YY, Tiinamaija T, Tsuang M, Turner D, Tusie-Luna T, Vartiainen E, Ware JS, Watkins H, Weersma RK, Wessman M, Wilson JG, Xavier RJ, Neale BM, Daly MJ, MacArthur DG, Genome Aggregation Database C, The mutational constraint spectrum quantified from variation in 141,456 humans. Nature 581, 434–443 (2020). [PubMed: 32461654]
18. McWilliam HEG, Eckle SBG, Theodossis A, Liu LG, Chen ZJ, Wubben JM, Fairlie DP, Strugnell RA, Mintern JD, McCluskey J, Rossjohn J, Villadangos JA, The intracellular pathway for the presentation of vitamin B-related antigens by the antigen-presenting molecule MR1. Nat Immunol 17, 531–537 (2016). [PubMed: 27043408]
19. Reantragoon R, Corbett AJ, Sakala IG, Gherardin NA, Furness JB, Chen ZJ, Eckle SBG, Uldrich AP, Birkinshaw RW, Patel O, Kostenko L, Meehan B, Kedzierska K, Liu LG, Fairlie DP, Hansen TH, Godfrey DI, Rossjohn J, McCluskey J, Kjer-Nielsen L, Antigen-loaded MR1 tetramers define T cell receptor heterogeneity in mucosal-associated invariant T cells. J Exp Med 210, 2305–2320 (2013). [PubMed: 24101382]
20. Alachkar H, Taubenheim N, Haeney MR, Durandy A, Arkwright PD, Memory switched B cell percentage and not serum immunoglobulin concentration is associated with clinical complications in children and adults with specific antibody deficiency and common variable immunodeficiency. Clin Immunol 120, 310–318 (2006). [PubMed: 16782407]

21. Heusinkveld LE, Majumdar S, Gao JL, McDermott DH, Murphy PM, WHIM Syndrome: from Pathogenesis Towards Personalized Medicine and Cure. J Clin Immunol 39, 532–556 (2019). [PubMed: 31313072]
22. Pastrana DV, Peretti A, Welch NL, Borgogna C, Olivero C, Badolato R, Notarangelo LD, Gariglio M, FitzGerald PC, McIntosh CE, Reeves J, Starrett GJ, Bliskovsky V, Velez D, Brownell I, Yarchoan R, Wyvill KM, Uldrick TS, Maldarelli F, Lisco A, Sereti I, Gonzalez CM, Androphy EJ, McBride AA, Van Doorslaer K, Garcia F, Dvoretzky I, Liu JS, Han J, Murphy PM, McDermott DH, Buck CB, Metagenomic Discovery of 83 New Human Papillomavirus Types in Patients with Immunodeficiency. mSphere 3, e00645–00618 (2018). [PubMed: 30541782]
23. Davey MS, Willcox CR, Hunter S, Kasatskaya SA, Remmerswaal EBM, Salim M, Mohammed F, Bemelman FJ, Chudakov DM, Oo YH, Willcox BE, The human Vδ2(+) T-cell compartment comprises distinct innate-like Vγ9(+) and adaptive Vγ9(−) subsets. Nat Commun 9, 1760 (2018). [PubMed: 29720665]
24. Wilson RP, Ives ML, Rao G, Lau A, Payne K, Kobayashi M, Arkwright PD, Peake J, Wong M, Adelstein S, Smart JM, French MA, Fulcher DA, Picard C, Bustamante J, Boisson-Dupuis S, Gray P, Stepensky P, Warnatz K, Freeman AF, Rossjohn J, McCluskey J, Holland SM, Casanova JL, Uzel G, Ma CS, Tangye SG, Deenick EK, STAT3 is a critical cell-intrinsic regulator of human unconventional T cell numbers and function. J Exp Med 212, 855–864 (2015). [PubMed: 25941256]
25. Martinez-Barricarte R, Markle JG, Ma CS, Deenick EK, Ramirez-Alejo N, Mele F, Latorre D, Mahdaviani SA, Aytekin C, Mansouri D, Bryant VL, Jabot-Hanin F, Deswarte C, Nieto-Patlan A, Surace L, Kerner G, Itan Y, Jovic S, Avery DT, Wong N, Rao G, Patin E, Okada S, Bigio B, Boisson B, Rapaport F, Seeleuthner Y, Schmidt M, Ikinciogullari A, Dogu F, Tanir G, Tabarsi P, Bloursaz MR, Joseph JK, Heer A, Kong XF, Migaud M, Lazarov T, Geissmann F, Fleckenstein B, Arlehamn CL, Sette A, Puel A, Emile JF, van de Vosse E, Quintana-Murci L, Di Santo JP, Abel L, Boisson-Dupuis S, Bustamante J, Tangye SG, Sallusto F, Casanova JL, Human IFN-gamma immunity to mycobacteria is governed by both IL-12 and IL-23. Sci Immunol 3, eaau6759 (2018). [PubMed: 30578351]
26. Okada S, Markle JG, Deenick EK, Mele F, Averbuch D, Lagos M, Alzahrani M, Al-Muhsen S, Halwani R, Ma CS, Wong N, Soudais C, Henderson LA, Marzouqa H, Shamma J, Gonzalez M, Martinez-Barricarte R, Okada C, Avery DT, Latorre D, Deswarte C, Jabot-Hanin F, Torrado E, Fountain J, Belkadi A, Itan Y, Boisson B, Migaud M, Arlehamn CSL, Sette A, Breton S, McCluskey J, Rossjohn J, de Villartay JP, Moshous D, Hambleton S, Latour S, Arkwright PD, Picard C, Lantz O, Engelhard D, Kobayashi M, Abel L, Cooper AM, Notarangelo LD, Boisson-Dupuis S, Puel A, Sallusto F, Bustamante J, Tangye SG, Casanova JL, IMMUNODEFICIENCIES. Impairment of immunity to Candida and Mycobacterium in humans with bi-allelic RORC mutations. Science 349, 606–613 (2015). [PubMed: 26160376]
27. Legoux F, Bellet D, Daviaud C, El Morr Y, Darbois A, Niort K, Procopio E, Salou M, Gilet J, Ryffel B, Balvay A, Foussier A, Sarkis M, El Marjou A, Schmidt F, Rabot S, Lantz O, Microbial metabolites control the thymic development of mucosal-associated invariant T cells. Science 366, 494–499 (2019). [PubMed: 31467190]
28. Gutierrez-Arcelus M, Teslovich N, Mola AR, Polidoro RB, Nathan A, Kim H, Hannes S, Slowikowski K, Watts GFM, Korsunsky I, Brenner MB, Raychaudhuri S, Brennan PJ, Lymphocyte innateness defined by transcriptional states reflects a balance between proliferation and effector functions. Nat Commun 10, 687 (2019). [PubMed: 30737409]
29. Koay HF, Gherardin NA, Enders A, Loh L, Mackay LK, Almeida CF, Russ BE, Nold-Petry CA, Nold MF, Bedoui S, Chen Z, Corbett AJ, Eckle SB, Meehan B, d'Udekem Y, Konstantinov IE, Lappas M, Liu L, Goodnow CC, Fairlie DP, Rossjohn J, Chong MM, Kedzierska K, Berzins SP, Belz GT, McCluskey J, Uldrich AP, Godfrey DI, Pellicci DG, A three-stage intrathymic development pathway for the mucosal-associated invariant T cell lineage. Nat Immunol 17, 1300–1311 (2016). [PubMed: 27668799]
30. Papadopoulou M, Tieppo P, McGovern N, Gosselin F, Chan JKY, Goetgeluk G, Dauby N, Cogan A, Donner C, Ginhoux F, Vandekerckhove B, Vermijlen D, TCR Sequencing Reveals the Distinct Development of Fetal and Adult Human Vγ9Vδ2 T Cells. J Immunol 203, 1468–1479 (2019). [PubMed: 31413106]

31. Leiding JW, Holland SM, Warts and all: human papillomavirus in primary immunodeficiencies. J Allergy Clin Immunol 130, 1030–1048 (2012). [PubMed: 23036745]
32. Stanley M, Immune responses to human papillomavirus. Vaccine 24 Suppl 1, S16–22 (2006). [PubMed: 16219398]
33. Krecke N, Smola S, Vogt T, Muller CSL, HPV-47-Induced and Tattoo-associated Verrucae Planae: Report of a Case and Review of the Literature. Dermatol Ther (Heidelb) 7, 549–554 (2017). [PubMed: 28836173]
34. Kirchhof MG, Wong SM, Tattoos and human papilloma virus: A case report of tattoo-associated flat warts (verrucae planae). SAGE Open Med Case Rep 7, 2050313X19857416 (2019).
35. Field MA, Cho V, Andrews TD, Goodnow CC, Reliably Detecting Clinically Important Variants Requires Both Combined Variant Calls and Optimized Filtering Strategies. Plos One 10, e0143199 (2015). [PubMed: 26600436]
36. Huang SX, Gilfillan S, Cella M, Miley MJ, Lantz O, Lybarger L, Fremont DH, Hansen TH, Evidence for MR1 antigen presentation to mucosal-associated invariant T cells. J Biol Chem 280, 21183–21193 (2005). [PubMed: 15802267]
37. Reantragoon R, Kjer-Nielsen L, Patel O, Chen ZJ, Illing PT, Bhati M, Kostenko L, Bharadwaj M, Meehan B, Hansen TH, Godfrey DI, Rossjohn J, McCluskey J, Structural insight into MR1-mediated recognition of the mucosal associated invariant T cell receptor. J Exp Med 209, 761–774 (2012). [PubMed: 22412157]
38. Patel O, Kjer-Nielsen L, Le Nours J, Eckle SB, Birkinshaw R, Beddoe T, Corbett AJ, Liu L, Miles JJ, Meehan B, Reantragoon R, Sandoval-Romero ML, Sullivan LC, Brooks AG, Chen Z, Fairlie DP, McCluskey J, Rossjohn J, Recognition of vitamin B metabolites by mucosal-associated invariant T cells. Nat Commun 4, 2142 (2013). [PubMed: 23846752]
39. Eckle SB, Birkinshaw RW, Kostenko L, Corbett AJ, McWilliam HE, Reantragoon R, Chen Z, Gherardin NA, Beddoe T, Liu L, Patel O, Meehan B, Fairlie DP, Villadangos JA, Godfrey DI, Kjer-Nielsen L, McCluskey J, Rossjohn J, A molecular basis underpinning the T cell receptor heterogeneity of mucosal-associated invariant T cells. J Exp Med 211, 1585–1600 (2014). [PubMed: 25049336]
40. Kabsch W, Xds. Acta Crystallogr D Biol Crystallogr 66, 125–132 (2010). [PubMed: 20124692]
41. Winn MD, Ballard CC, Cowtan KD, Dodson EJ, Emsley P, Evans PR, Keegan RM, Krissinel EB, Leslie AG, McCoy A, McNicholas SJ, Murshudov GN, Pannu NS, Potterton EA, Powell HR, Read RJ, Vagin A, Wilson KS, Overview of the CCP4 suite and current developments. Acta Crystallogr D Biol Crystallogr 67, 235–242 (2011). [PubMed: 21460441]
42. Adams PD, Afonine PV, Bunkoczi G, Chen VB, Davis IW, Echols N, Headd JJ, Hung LW, Kapral GJ, Grosse-Kunstleve RW, McCoy AJ, Moriarty NW, Oeffner R, Read RJ, Richardson DC, Richardson JS, Terwilliger TC, Zwart PH, PHENIX: a comprehensive Python-based system for macromolecular structure solution. Acta Crystallogr D Biol Crystallogr 66, 213–221 (2010). [PubMed: 20124702]
43. McCoy AJ, Solving structures of protein complexes by molecular replacement with Phaser. Acta Crystallogr D Biol Crystallogr 63, 32–41 (2007). [PubMed: 17164524]
44. Emsley P, Cowtan K, Coot: model-building tools for molecular graphics. Acta Crystallogr D Biol Crystallogr 60, 2126–2132 (2004). [PubMed: 15572765]
45. Chen VB, Arendall WB 3rd, Headd JJ, Keedy DA, Immormino RM, Kapral GJ, Murray LW, Richardson JS, Richardson DC, MolProbity: all-atom structure validation for macromolecular crystallography. Acta Crystallogr D Biol Crystallogr 66, 12–21 (2010). [PubMed: 20057044]
46. Reuter A, Panozza SE, Macri C, Dumont C, Li J, Liu H, Segura E, Vega-Ramos J, Gupta N, Caminschi I, Villadangos JA, Johnston AP, Mintern JD, Criteria for dendritic cell receptor selection for efficient antibody-targeted vaccination. J Immunol 194, 2696–2705 (2015). [PubMed: 25653426]
47. Wang C, Sanders CM, Yang Q, Schroeder HW Jr., Wang E, Babrzadeh F, Gharizadeh B, Myers RM, Hudson JR Jr., Davis RW, Han J, High throughput sequencing reveals a complex pattern of dynamic interrelationships among human T cell subsets. Proc Natl Acad Sci U S A 107, 1518–1523 (2010). [PubMed: 20080641]

48. Han J, Swan DC, Smith SJ, Lum SH, Sefers SE, Unger ER, Tang YW, Simultaneous amplification and identification of 25 human papillomavirus types with Templex technology. J Clin Microbiol 44, 4157–4162 (2006). [PubMed: 17005760]

49. Wu B, Peisley A, Richards C, Yao H, Zeng X, Lin C, Chu F, Walz T, Hur S, Structural basis for dsRNA recognition, filament formation, and antiviral signal activation by MDA5. Cell 152, 276–289 (2013). [PubMed: 23273991]

50. Zaki M, Thoenes M, Kawalia A, Nurnberg P, Kaiser R, Heller R, Bolz HJ, Recurrent and Prolonged Infections in a Child with a Homozygous IFIH1 Nonsense Mutation. Front Genet 8, 130 (2017). [PubMed: 29018476]

51. Lamborn IT, Jing H, Zhang Y, Drutman SB, Abbott JK, Munir S, Bade S, Murdock HM, Santos CP, Brock LG, Masutani E, Fordjour EY, McElwee JJ, Hughes JD, Nichols DP, Belkadi A, Oler AJ, Happel CS, Matthews HF, Abel L, Collins PL, Subbarao K, Gelfand EW, Ciancanelli MJ, Casanova JL, Su HC, Recurrent rhinovirus infections in a child with inherited MDA5 deficiency. J Exp Med 214, 1949–1972 (2017). [PubMed: 28606988]

52. Le Nours J, Gherardin NA, Ramarathinam SH, Awad W, Wiede F, Gully BS, Khandokar Y, Praveena T, Wubben JM, Sandow JJ, Webb AI, von Borstel A, Rice MT, Redmond SJ, Seneviratna R, Sandoval-Romero ML, Li S, Souter MNT, Eckle SBG, Corbett AJ, Reid HH, Liu L, Fairlie DP, Giles EM, Westall GP, Tothill RW, Davey MS, Berry R, Tiganis T, McCluskey J, Pellicci DG, Purcell AW, Uldrich AP, Godfrey DI, Rossjohn J, A class of gammadelta T cell receptors recognize the underside of the antigen-presenting molecule MR1. Science 366, 1522–1527 (2019). [PubMed: 31857486]

53. Dati F, Schumann G, Thomas L, Aguzzi F, Baudner S, Bienvenu J, Blaabjerg O, Blirup-Jensen S, Carlstrom A, Petersen PH, Johnson AM, Milford-Ward A, Ritchie RF, Svendsen PJ, Whicher J, Consensus of a group of professional societies and diagnostic companies on guidelines for interim reference ranges for 14 proteins in serum based on the standardization against the IFCC/BCR/CAP Reference Material (CRM 470). International Federation of Clinical Chemistry. Community Bureau of Reference of the Commission of the European Communities. College of American Pathologists. Eur J Clin Chem Clin Biochem 34, 517–520 (1996). [PubMed: 8831057]

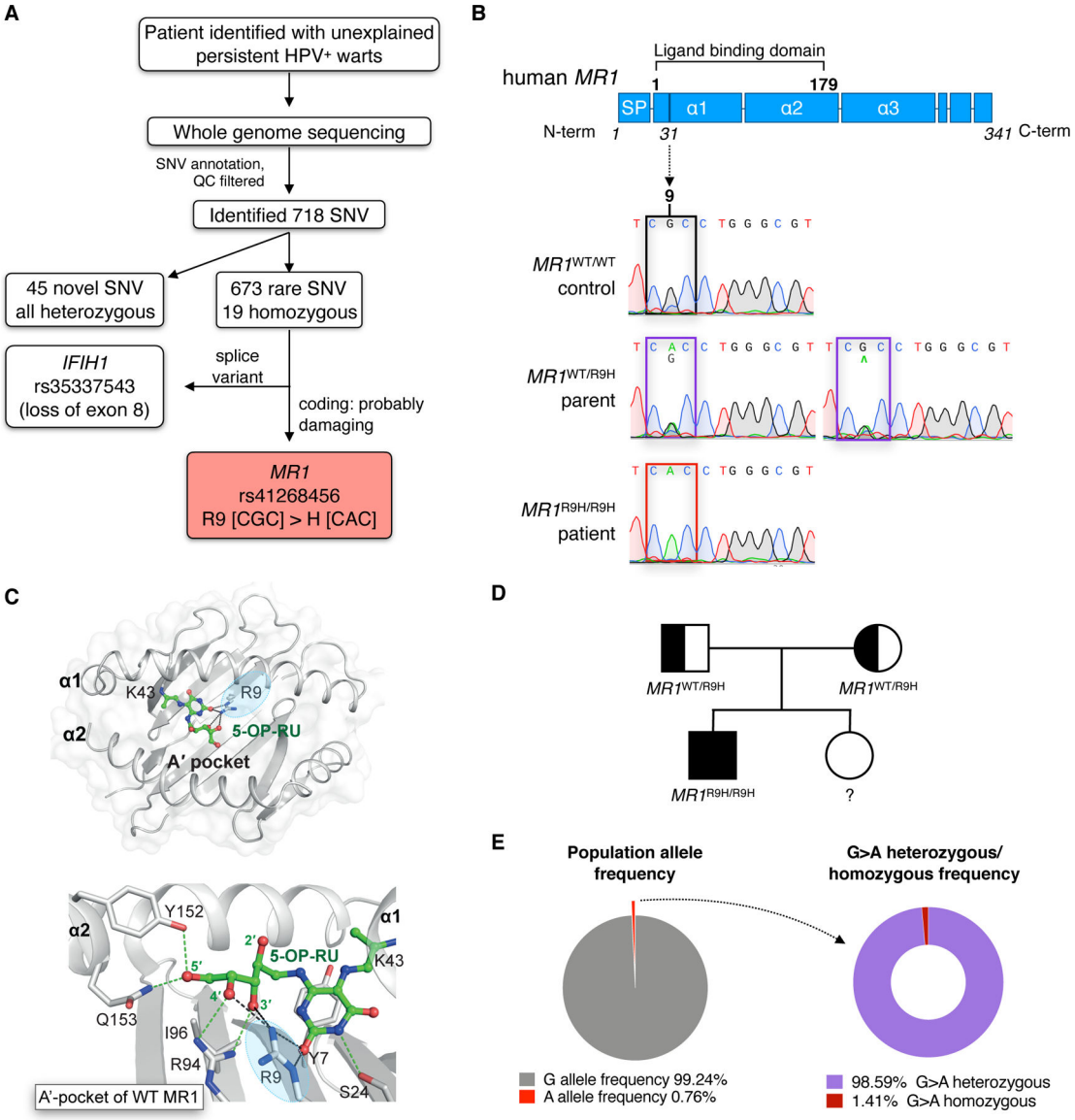

Fig. 1. Whole exome analysis reveals rare homozygous missense SNV rs41268456 in *MR1*.

(**A**) Diagram showing whole exome sequencing results for a patient with persistent HPV infection. For full SNV list see Table S1 and S2. QC, quality control; SNV, single nucleotide variance. (**B**) Graphical representation of the MR1 protein, line shows location of the point mutation at position 9 of the ligand-binding pocket of MR1. SP, signal peptide. Sanger sequencing results confirm the G>A substitution in the patient's *MR1* gene compared to a wild-type (WT) control and heterozygous parent. (**C**) The ligand-binding pocket of WT MR1 (PDB: 6PUC) showing how R9 (circled in blue) interactions stabilise 5-(2-oxopropylideneamino)-6-D-ribitylaminouracil (5-OP-RU) within the A'-pocket. MR1 helices, sheets, and residues are shown in grey, and 5-OP-RU is shown as green sticks. H-bonds are shown as green dashes, except for R9 mediated H-bonds that are shown as black dashes. (**D**) Familial segregation of the $MR1^{R9H}$ mutation in a non-consanguineous Australian family. (**E**) Population frequency of rs41268456 and the

proportion of heterozygous vs homozygous individuals. Values based on data accessed via the online Genome Aggregation Database (gnomAD) (17).

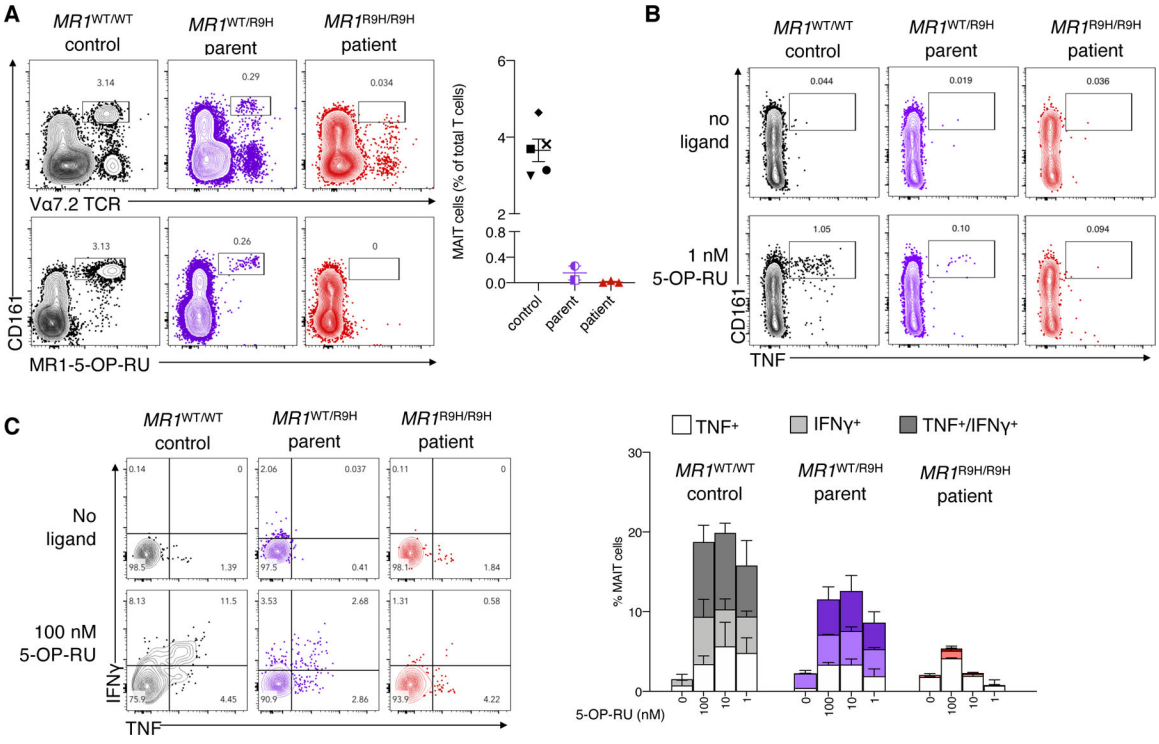

Fig. 2. MR1$^{R9H/R9H}$ patient lacks MAIT cells and their antigen presenting cells cannot activate in an MR1-restricted manner.

Analysis of MAIT cells in peripheral blood mononuclear cells (PBMC) from *MR1*$^{WT/WT}$ controls (n = 3–5, age/gender matched to patient), *MR1*$^{WT/R9H}$ parents (n = 2) and *MR1*$^{R9H/R9H}$ patient (n = 1, two or three timepoints, three months apart) (**A**) Representative flow cytometry plots showing circulating MAIT cells. Cells are gated on the CD3$^+$ T cell receptor (TCR)αβ$^+$ TCRγδ$^-$ population, and MAIT cells identified by the surrogate markers Vα7.2$^+$ CD161$^+$ or by the MR1 5-OP-RU loaded tetramer. Graph shows the frequency of MAIT cells (Va7.2$^+$ CD161$^+$ MR1 5-OP-RU tetramer$^+$). (**B**) Representative flow cytometry plots of TNF production by PBMC (gated on CD3$^+$ TCRαβ$^+$ TCRγδ$^-$ population) when cultured with 1 nM 5-OP-RU and brefeldin A (BFA) for 18 hr. (**C**) Allogeneic MAIT cell activation coculture, where *MR1*$^{WT/WT}$ control B cells (n = 2), *MR1*$^{WT/R9H}$ parent B cells (n = 2) or *MR1*$^{R9H/R9H}$ patient B cells (n = 1, two time points, three months apart) were pre-incubated for 4 hr with indicated concentrations of 5-OP-RU. Cells were washed, BFA added and cocultured with allogeneic healthy donor T cells for 18 hr. Cytokine production by CD3$^+$ Vα7.2$^+$ CD161$^+$ cells was then measured by intracellular staining for TNF and IFNγ. </Figure_caption>

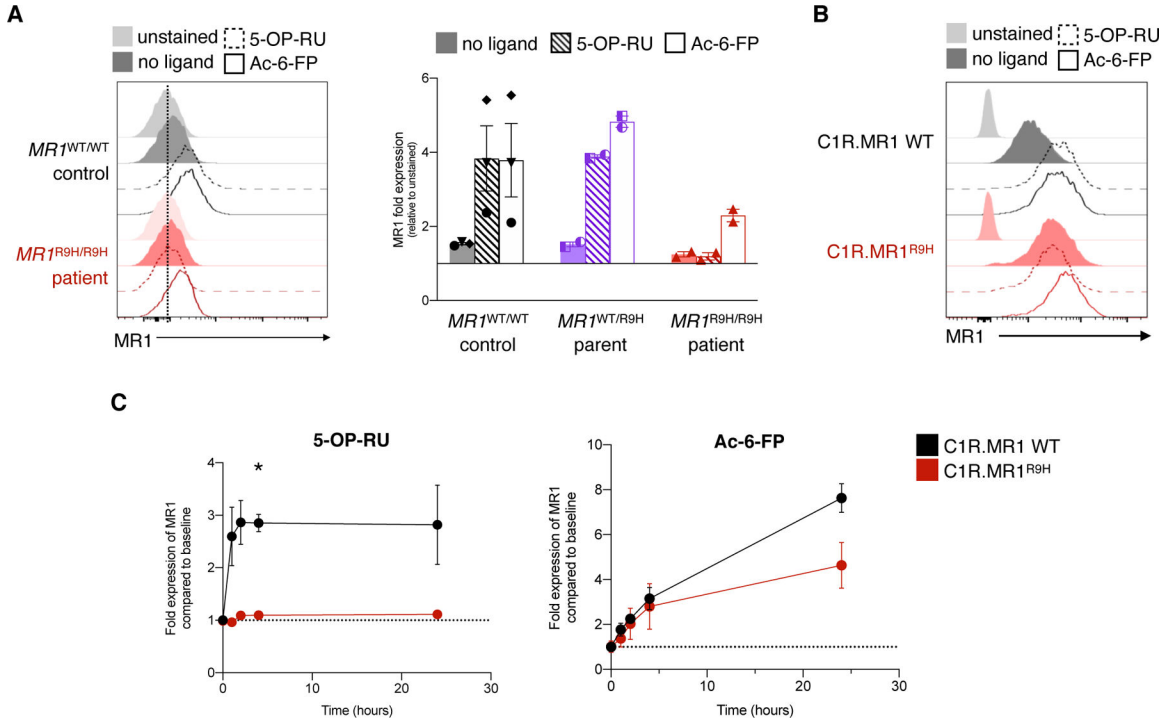

Fig. 3. MR1^{R9H} does not upregulate in response to 5-OP-RU.

(**A**) Histogram and graph showing the expression of MR1 on CD19^{+} B cells. PBMC were incubated with acetyl-6-formylpterin (Ac-6-FP) (10 μM) or 5-OP-RU (1 μM) for 4 hr and then stained with 8F2.F9 MR1 antibody and anti-CD19. Each symbol in a graph represents an individual, line is at mean and error bars represent standard error (SE). (**B**) Histogram shows MR1 expression on C1R.MR1 WT and C1R.MR1^{R9H} cell lines after addition of Ac-6-FP (10 μM) or 5-OP-RU (1 μM) and incubation for 4 hr. (**C**) MR1 upregulation time course assay showing the dynamics of MR1 upregulation after addition of Ac-6-FP (10 μM) or 5-OP-RU (1 μM) on C1R.MR1 WT and C1R.MR1^{R9H} over 24 hr. Each point represents mean between three independent experiments and error bars represent SE. Statistical significance calculated using two-way ANOVA with Geisser-Greenhouse correction and Sidak's multiple comparison test, where *$P < 0.05$. See Fig. S4 for flow cytometry gating strategies.</Figure_caption>

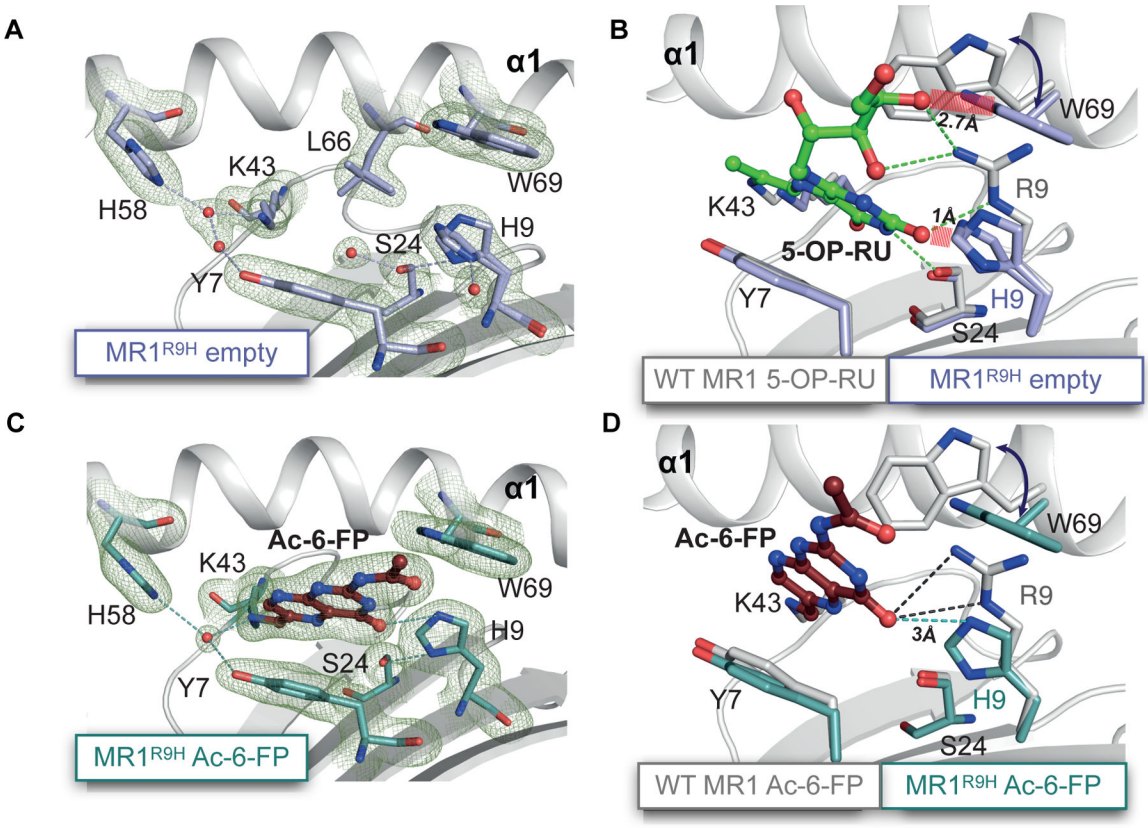

Fig. 4. R9H mutation causes structural changes to the ligand-binding pocket of MR1.

The crystal structures of the ligand-binding pocket of WT MR1 and MR1^{R9H}. (**A**) MR1^{R9H}-empty and (**B**) MR1^{R9H}-Ac-6-FP, of the ternary MAIT TCR-MR1^{R9H} complexes. Maps were prepared using the phenix-refine crystallographic structure refinement program and presented as an $2F_o-F_c$ map (observed structure factor − calculated structure factor; mesh) contoured at 1σ. (**C**) Superposition of the ligand-binding pocket of WT MR1 5-OP-RU (PDB: 6PUC(16)) and MR1^{R9H}-empty, arrow shows the new orientation of W69, steric clashes between 5-OP-RU conformation in WT MR1 and MR1^{R9H}-empty structure are shown as red dashes. (**D**) Superposition of the ligand-binding pocket of WT MR1 Ac-6-FP (PDB; 4PJ5(39)) and MR1^{R9H} Ac-6-FP, showing similar binding of Ac-6-FP within the pocket. Ac-6-FP and 5-OP-RU ligands are shown as ruby and green sticks, respectively. Water molecules are shown as red spheres and hydrogen bonding is shown as dashed lines. </Figure_caption>

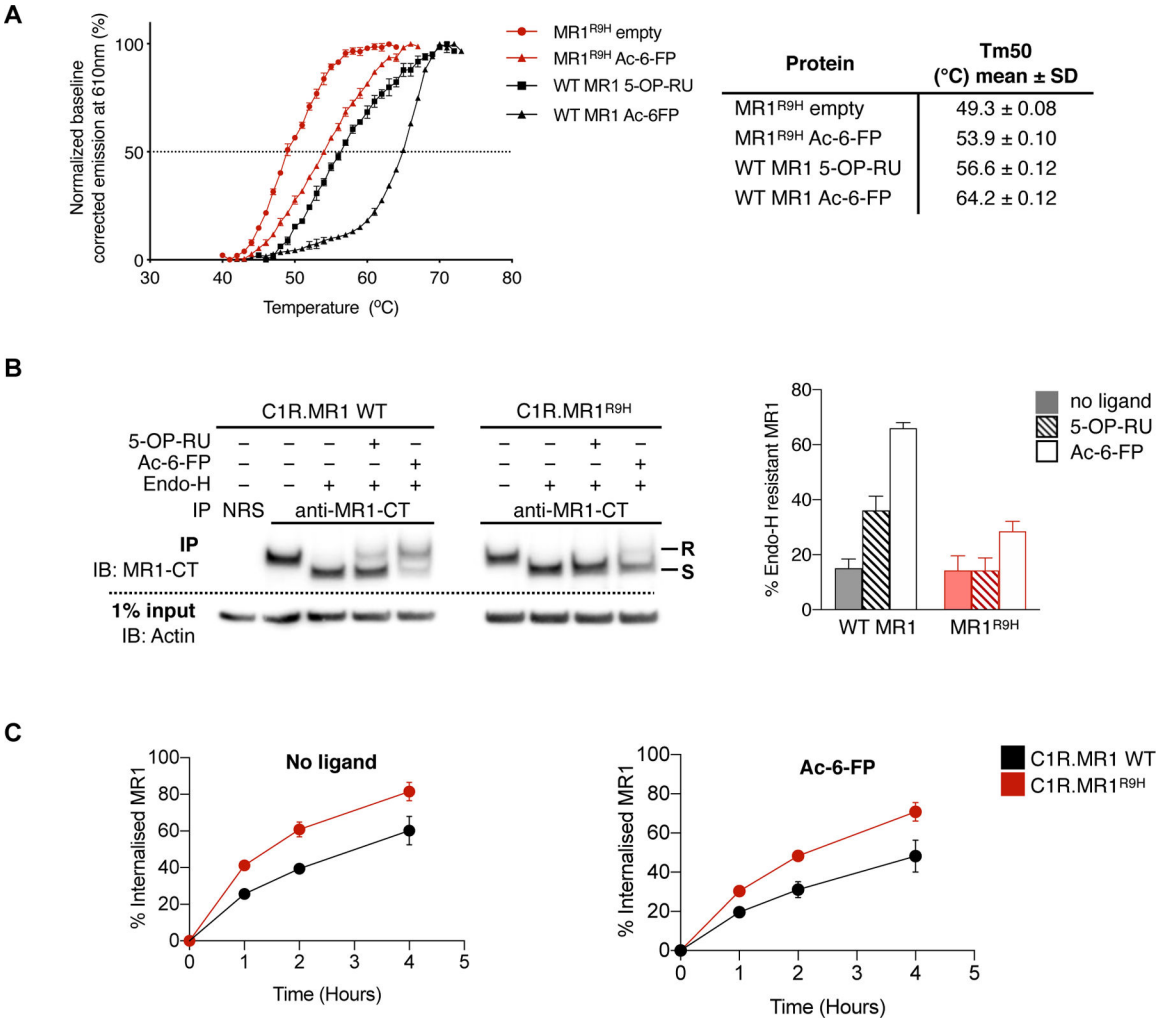

Protein	Tm50 (°C) mean ± SD
MR1R9H empty	49.3 ± 0.08
MR1R9H Ac-6-FP	53.9 ± 0.10
WT MR1 5-OP-RU	56.6 ± 0.12
WT MR1 Ac-6-FP	64.2 ± 0.12

Fig. 5. The R9H mutation impacts the stability and cellular trafficking of MR1.

(**A**) Thermostability of soluble WT MR1 and MR1^{R9H} as measured by fluorescence-based thermal shift assay. Graph shows baseline-corrected, normalized emission at 610 nm plotted against temperature (°C) and Boltzmann curve-fits. Each point represents the mean of three technical replicates and error bars represent SD. The half maximum melting point (Tm50) is represented as a dotted line. Table shows the mean Tm50 across three independent experiments, each measured in at least technical duplicate. Data are representative of three independent experiments. (**B**) C1R cells transduced with either WT MR1 or MR1^{R9H} were cultured alone or with 2 μM 5-OP-RU or Ac-6-FP for 5 hr. MR1 was immunoprecipitated (IP) using anti-MR1-CT or normal rabbit serum (NRS) as a control, treated with or without endoglycosidase H (endo-H) and then immunoblotted (IB) for MR1 and actin. Graph shows the amount of endo-H-resistant MR1 determined by densitometry and calculated as a percentage of the total MR1 for each IP. Graph bars represent mean of four independent experiments and error bars represent SEM. S, endo-H-sensitive; R, endo-H-resistant. (**C**) C1R.MR1 WT or C1R.MR1^{R9H} cell lines were cultured alone or with 10μM Ac-6-FP overnight. The amount of internalized MR1 was measured using a fluorescence

internalisation probe (FIP) conjugated to anti-MR1 8F2.F9 antibody. Each point represents the mean of two independent experiments and error bars represent SD.</Figure_caption>

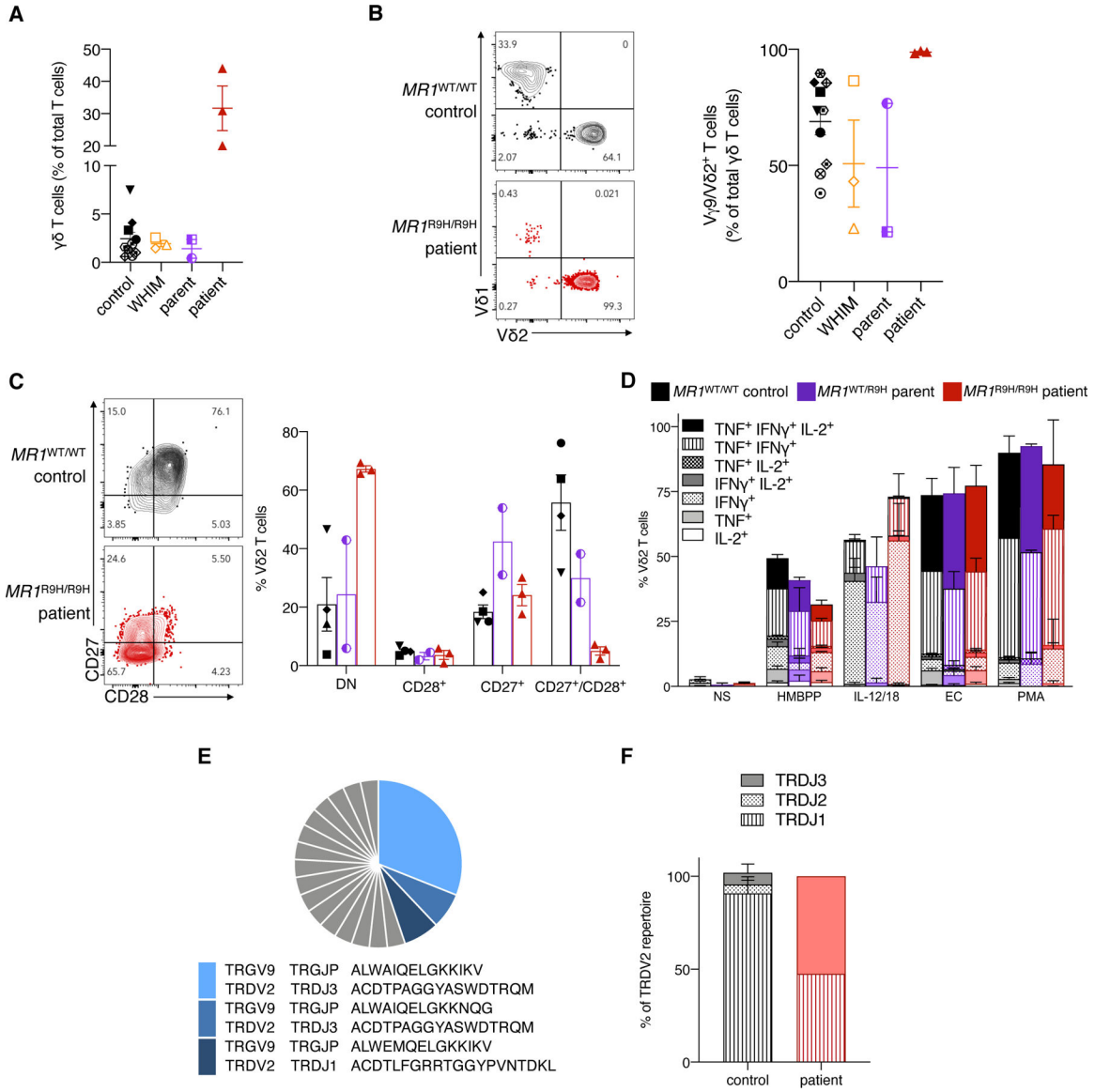

Fig. 6. *MR1*$^{R9H/R9H}$ patient has a highly expanded circulating Vδ2 γδ T cell population

(**A**) Graph showing the frequency of circulating γδ T cells as a proportion of total T cells for controls (n = 4, age/gender matched to *MR1*$^{R9H/R9H}$ patient solid symbols, n = 6 age matched to WHIM patients open symbols), WHIM HPV^{+} patients (n = 3), *MR1*$^{WT/R9H}$ parents (n = 2) and *MR1*$^{R9H/R9H}$ patient (n = 1, three timepoints, three months apart). (**B**) Representative flow cytometry plots showing circulating frequency of Vδ1 and Vδ2 as a percentage of the γδ T cell population in *MR1*$^{WT/WT}$ controls (n = 4) *MR1*$^{WT/R9H}$ parents (n = 2) and *MR1*$^{R9H/R9H}$ patient (n = 1, three timepoints, three months apart). Graph shows the frequency of Vγ9/Vδ2^{+} as a proportion of total γδ T cells. (**C**) Representative flow cytometry plots showing the frequency of Vδ2 T cells expressing CD27 and CD28. Graph shows the frequency of Vδ2^{+} γδ T cells that are CD27^{-}/CD28^{-} (DN), CD27^{-}/CD28^{+}, CD27^{+}/CD28^{-}, and CD27^{+}/CD28^{+}. (**D**) Activation assay examining the Vδ2^{+} γδ T cell cytokine production in *MR1*$^{WT/WT}$ controls (n = 4) *MR1*$^{WT/R9H}$ parents (n = 2)

and *MR1*$^{R9H/R9H}$ patient (n = 1, two timepoints, three months apart). Response to various stimuli is measured by intracellular staining for IL-2, TNF and IFNγ after 18 hr stimulation in the presence of BFA. Graph shows stacked results where bar is at mean for each cytokine combination and error bars represent SE. (**E**) Vδ2^{+} γδ T cell clones revealed by single cell multiplex PCR sequencing from the *MR1*$^{R9H/R9H}$ patient. Clones that were identified once are coloured grey and clones that were identified multiple times are coloured blue and their CDR3γ and CDR3δ sequences listed. (**F**) Graph of the TRDJ usage by Vγ9/Vδ2^{+} T cells in healthy controls (n = 3) compared to *MR1*$^{R9H/R9H}$ patient (n = 1).</Figure_caption>

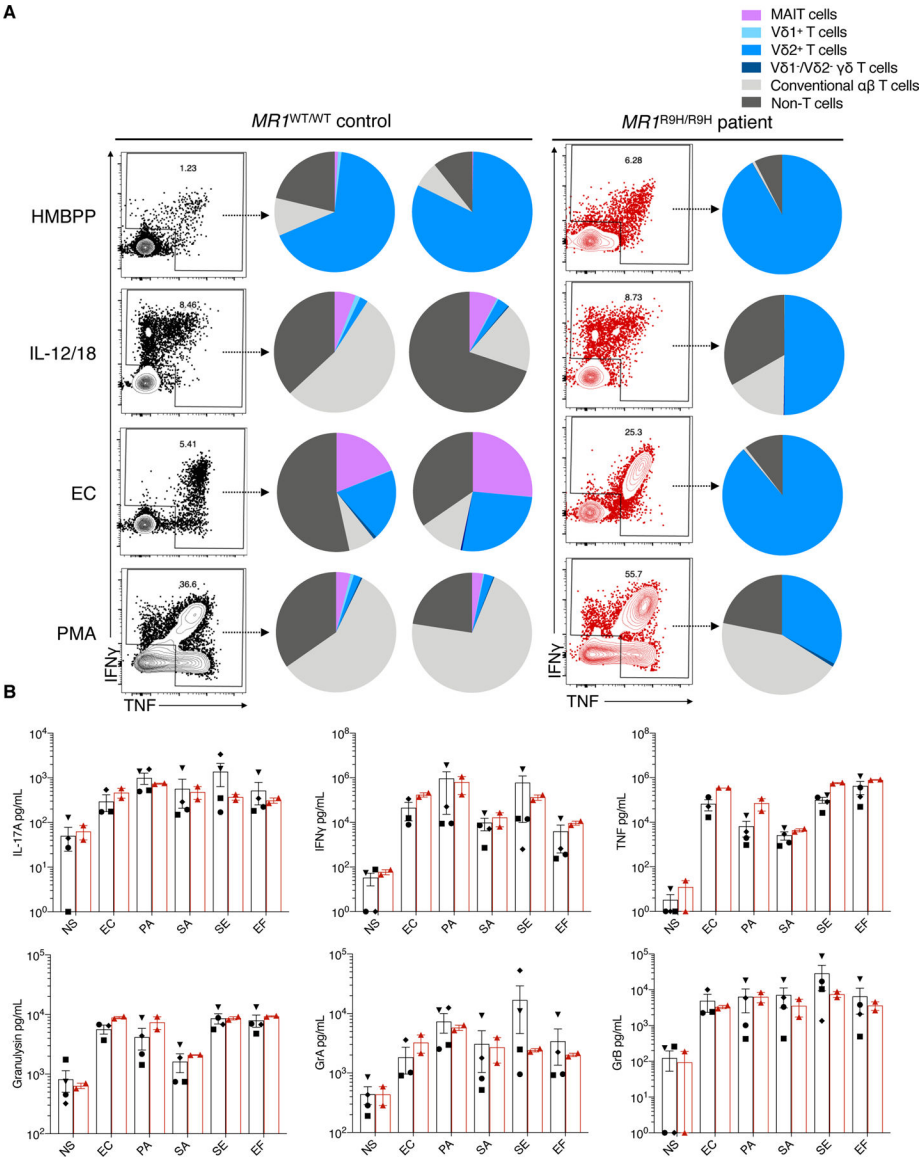

Fig. 7. MR1$^{R9H/R9H}$ patient's Vδ2^{+} γδ T cell population compensates functionally for the lack of MAIT cells during ex vivo bacterial challenge

(**A**) Plots show the total TNF and IFNγ production by live PBMC in response to various stimuli as measured by intracellular staining for TNF and IFNγ after 18 hr stimulation in the presence of BFA. Pie charts show the proportions of each cell type contributing to the TNF and/or IFNγ production. HMBPP, (E)-4-Hydroxy-3-methyl-but-2-enyl pyrophosphate 10 ng/mL; IL-12/IL-18, two doses of 200 ng/mL with IL-2 (100 U/mL) that were added 72 hr apart; EC, *E. coli* MOI 50; PMA, phorbol 12-myristate 13-acetate (50 ng/mL) and ionomycin (1 μg/mL). (**B**) Graphs showing the concentration of cytokines and cytotoxic molecules measured used LEGENDplex™ CD8/NK panel by PBMC from *MR1*$^{WT/WT}$ control (n = 3–4) and *MR1*$^{R9H/R9H}$ patient (n = 1, two timepoints, 3 months apart) when cultured with various bacteria MOI 50 for 24 hr. NS, no stimulation; EC, *E. coli*; PA, *Pseudomonas aeruginosa*; SA, *Staphylococcus aureus*; SE, *Staphylococcus epidermidis*; EF,

Enterococcus faecalis; Gr, granzyme. Each symbol in a graph represents an individual, bar is at mean and error bars represent SEM.</Figure_caption>